International Journal of Digital Earth
Publication details, including instructions for authors and subscription information:
http://www.informaworld.com/smpp/title~content=t777764757

Arithmetic and Fourier transform for the PYXIS multi-resolution digital Earth model

A. Vince [a]; X. Zheng [b]
[a] Department of Mathematics, University of Florida, Gainesville, FL, USA [b] Department of Arts and Sciences, Voorhees College, Denmark, SC, USA

Online Publication Date: 01 March 2009

To cite this Article Vince, A. and Zheng, X.(2009)'Arithmetic and Fourier transform for the PYXIS multi-resolution digital Earth model',International Journal of Digital Earth,2:1,59 — 79

To link to this Article: DOI: 10.1080/17538940802657694

URL: http://dx.doi.org/10.1080/17538940802657694

International Journal of Digital Earth,
Vol. 2, No. 1, March 2009, 59–79

Taylor & Francis
Taylor & Francis Group

Arithmetic and Fourier transform for the PYXIS multi-resolution digital Earth model

A. Vince[a]* and X. Zheng[b]

[a]*Department of Mathematics, University of Florida, Gainesville, FL 32611-8105, USA;*
[b]*Department of Arts and Sciences, Voorhees College, Denmark, SC 29042, USA*

(Received 6 March 2008; final version received 30 November 2008)

This paper investigates a multi-resolution digital Earth model called PYXIS, which was developed by PYXIS Innovation Inc. The PYXIS hexagonal grids employ an efficient hierarchical labeling scheme for addressing pixels. We provide a recursive definition of the PYXIS grids, a systematic approach to the labeling, an algorithm to add PYXIS labels, and a discussion of the discrete Fourier transform on PYXIS grids.

Keywords: discrete grid; digital Earth; Fourier transform

1. Introduction

The representation and analysis of global data has a history that dates back several millennia. The oldest known maps are preserved on Babylonian clay tablets from about 2300 B.C. The first whole world maps began to appear in the early 16th century, following voyages by Columbus and others to the New World. Buckminster Fuller invented the geodesic dome in the late 1940s. Geographic information systems (GIS) emerged in the 1970–1980s. The emphasis over the past few decades has been on the computer display and analysis of georeferenced information and remotely sensed data about the Earth. Traditional reference models of the Earth are based on the spherical coordinates of latitude and longitude, but recent models, called *discrete global grids* (DGGs), are based on cellular subdivisions of regular polyhedra (in particular, the tetrahedron, octahedron, and icosahedron).

There is a substantial recent literature on discrete global grids, including Ahuja (1983), Baumgardner and Frederickson (1985), Brodzik and Knowles (2002), Carr *et al*. (1992), Chen *et al*. (2003), Goodchild and Shiren (1992), Kidd (2005), Lee and Samet (1998), Sahr *et al*. (2003), Szalay *et al*. (2005), Tong *et al*. (2007), and Vince (2006). The most commonly used is the *icosahedral, aperture 3, multi-resolution, hexagonal discrete global grid*. The term *hexagonal* is used because the cells are hexagonal (except 12 pentagonal cells). While traditional image processing algorithms and digital image transforms are typically computed on rectangular grids, for many applications hexagonal grids are advantageous. Hexagonal grids have a high packing density, approximate circular regions, and each cell has equal distance from its six immediate neighbors. Hexagonal grids appear in a wide variety of

*Corresponding author. Email: avince@math.ufl.edu

ISSN 1753-8947 print/ISSN 1753-8955 online

DOI: 10.1080/17538940802657694
http://www.informaworld.com

applications such as image processing (Middleton and Sivaswamy 2005), geoscience (Carr *et al*. 1992), and the soil moisture and ocean salinity space mission (Camps *et al*. 1997, Anterrieu *et al*. 2002). The term *icosahedral* is used because the centers of the cells are located at the vertices of certain subdivisions of the icosahedron. The *Snyder equal area* method (Snyder 1992) is often used to project the subdivided icosahedron onto the surface of the sphere (no projection method can simultaneously preserve both area and angle). The icosahedral Snyder equal area aperture 3 hexagonal DGG is usually referred to as ISAE3H. *Multi-resolution* means that there is not just a single tessellation, but a hierarchical sequence of progressively finer tessellations. Going further in the sequence zooms in on smaller areas. *Aperture 3* refers to the approximate ratio between the areas of hexagons at successive tessellations in the sequence. In fact, this small ratio is one of the features that makes an aperture 3 DGG appealing. A high resolution of ISEA3H appears in Figure 1.

A major issue in any application of a discrete global grid is how to reference the cells, i.e. how to give each cell a useful label or address. This paper concentrates on a novel approach being developed by PYXIS Innovation, Inc., a company based in Kingston, Ontario, Canada. This paper concerns, not its performance compared with other digital Earth models, but three particular foundational issues. First, a precise mathematical description of the indexing system is provided in Section 3, together with a list of its properties. Second, basic to many DGG applications is an efficient algorithm for the vector addition of points in terms of their addresses. A linear time algorithm is provided in Section 4. Third, the discrete Fourier transform (DFT) is ubiquitous in data analysis (Dudgeon and Mersereau 1984). An approach that is applicable to the PYXIS grid is given in Section 5. Section 2 provides a summary of the PYXIS approach to the ISEA3H.

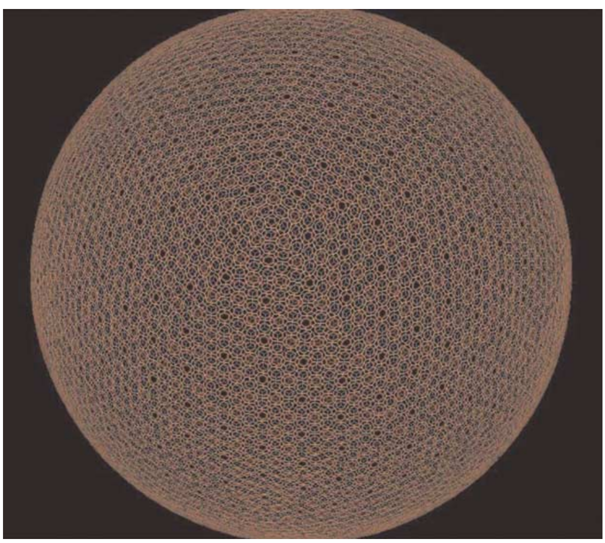

Figure 1. ISEA3H.

2. PYXIS approach

This section provides a summary of the PYXIS© approach to the ISEA3H. This approach is based on a partition of the sphere into 32 regions, each region modeled by a multi-resolution sequence of finite, planar, hexagonal grids. The brief summary of how these planar PYXIS© grids partition the sphere is meant as motivation for their use in a digital Earth setting. A more precise mathematical description of the PYXIS© grids is given in Section 3.

Finite, planar, hexagonal, multi-resolution grids with nice properties have previously appeared. In particular, Lucas (1979) described a multi-resolution sequence of planar, hexagonal grids called GBT_2 (general balanced ternary). Moreover, the cells in each grid in the sequence can be labeled in a natural way. This labeling has the property that labels can be added and multiplied conveniently, i.e. algebraically the structure is a ring (Kitto and Wilson 1991). Kitto *et al*. (1994) showed that this ring is isomorphic to the 7-adic integers. Zapata and Ritter (2000) developed a fast Fourier transform on GBT_2. Unfortunately, the generalized balanced ternary is not compatible with a spherical grid. The ISEA3H discrete global grid cannot be partitioned into (projected) copies of GBT_2.

The basis of the PYXIS© digital Earth reference model is a multi-resolution sequence $\mathbf{P}$ of planar hexagonal grids introduced by Peterson (2003) and PYXIS Innovation Inc. (2006). Let $\mathbf{P}_n$ denote the nth *level* or *resolution*, i.e. the nth grid in the sequence $\mathbf{P}$. Figures 2 and 3 show the hexagonal cells of $\mathbf{P}_1$ through $\mathbf{P}_4$. In Figure 2, the levels are superimposed.

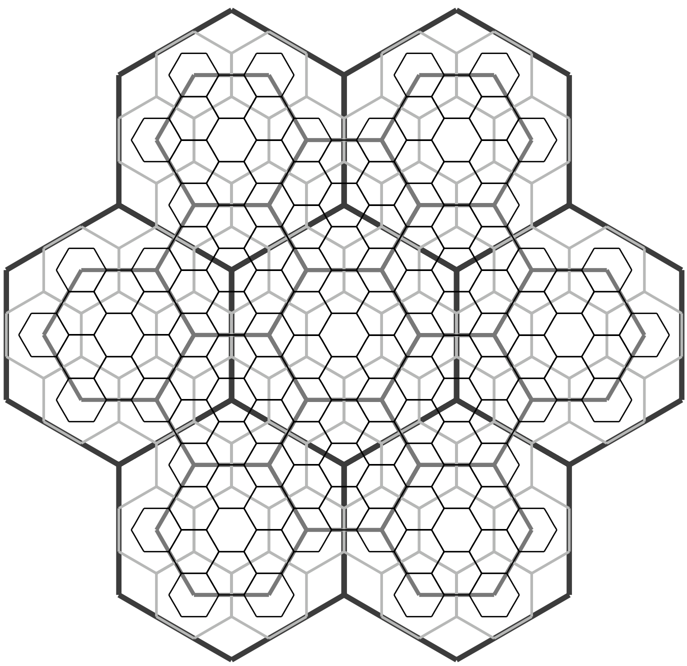

Figure 2. Levels 1 through 4 of the PYXIS array.

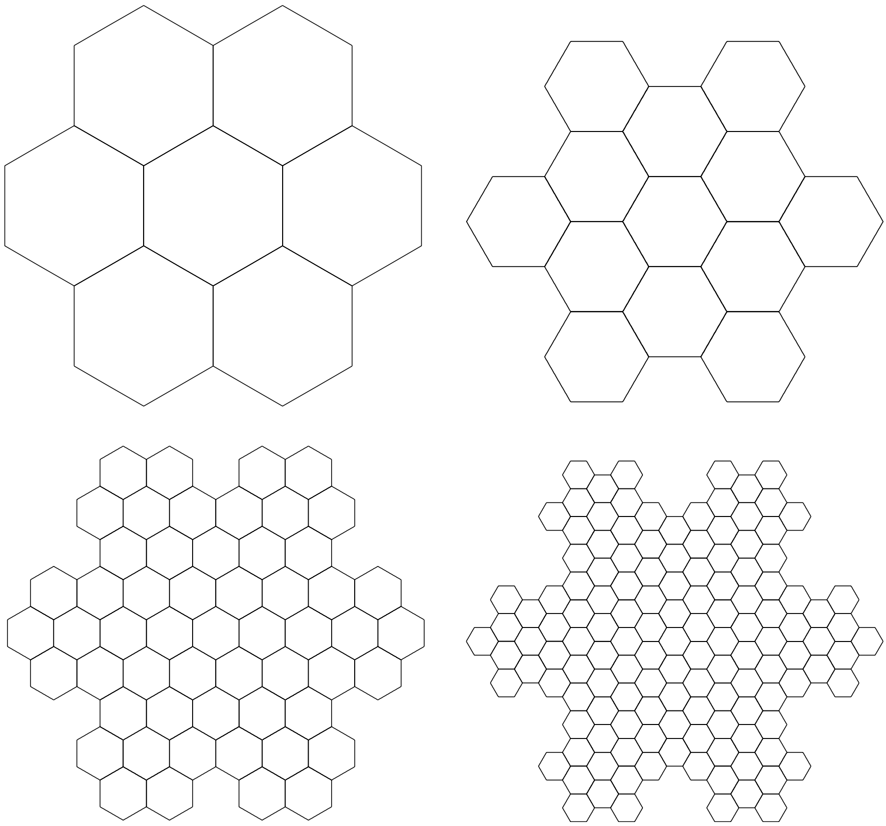

Figure 3. The first four grids in **P**, containing seven hexagons, 13 hexagons, 55 hexagons, and 133 hexagons, respectively.

A sketch of how the PYXIS© grids $\mathbf{P}_n$ are applied to the ISEA3H is as follows. The central fact is that, for each n, the nth resolution of the ISEA3H can basically be partitioned into 20 projected copies of $\mathbf{P}_{n-1}$ and 12 projected copies of $\mathbf{P}_n$. This is done recursively. The sphere is first tessellated by 20 hexagonal and 12 pentagonal regions as shown in Figure 4(a), where the sphere has been flattened onto the plane. Figure 4(b) shows each pentagon in Figure 4(a) as a hexagon with one of its six directions 'empty'. This allow us, for practical purposes, to treat each of the 12 pentagons at each level as a hexagon. For each edge of a polygon in Figure 4(b), construct a line segment $1/\sqrt{3}$ times the length of that edge and a perpendicular bisector of that edge. This results in the subdivision shown in Figure 5. Repeating this process again results in the finer resolution subdivision shown in Figure 6. Figure 4(b), 5, and 6 are the zeroth, first, and second level resolutions of the ISEA3H discrete global grid. As illustrated in Figure 6(right), the second resolution tessellation of the sphere is the non-overlapping union of 20 copies of $\mathbf{P}_1$ and 12 copies of $\mathbf{P}_2$ (by omitting one of its six directions). In general, the ISEA3H is the non-overlapping union of 20 projected copies of $\mathbf{P}_{n-1}$ and 12 projected copies of $\mathbf{P}_n$.

This section provided an informal introduction to the PYXIS© approach to the icosahedral, Snyder equal area, aperture 3, hexagonal discrete global grid in terms of

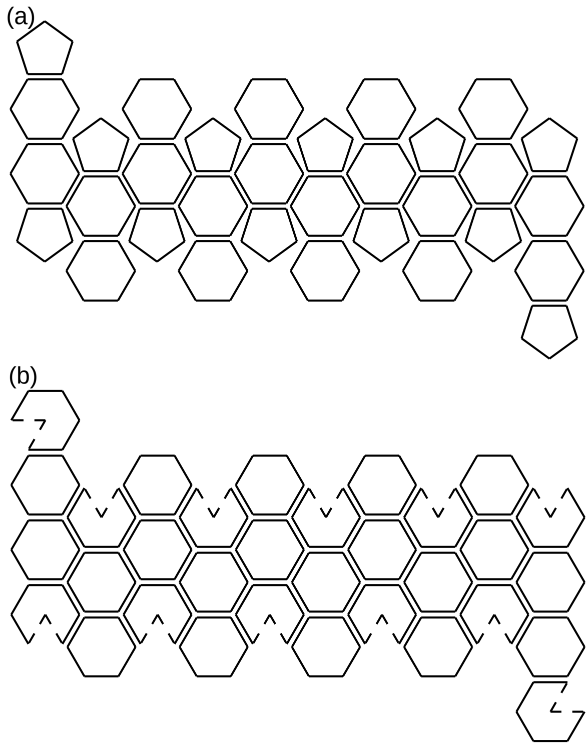

Figure 4. (a) The 20 hexagons and 12 pentagons in a tessellation of the flattened sphere. (b) Each pentagon in (a) as a hexagon with one of its six directions empty.

finite, planar, hexagonal grids denoted $\mathbf{P}_n$. The next section of this paper provides a precise recursive definition of the array $\mathbf{P}_n$ and also a systematic approach to the labeling of the cells of $\mathbf{P}_n$.

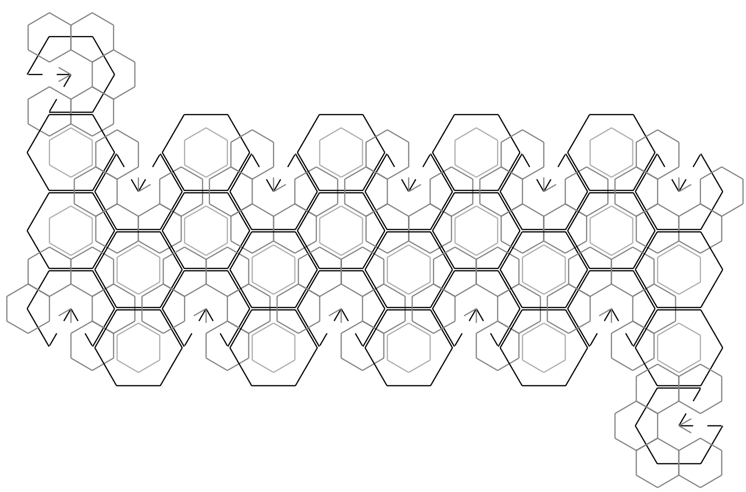

Figure 5. Level 1 – the polygons obtained from the subdivision of polygons in Figure 4(b).

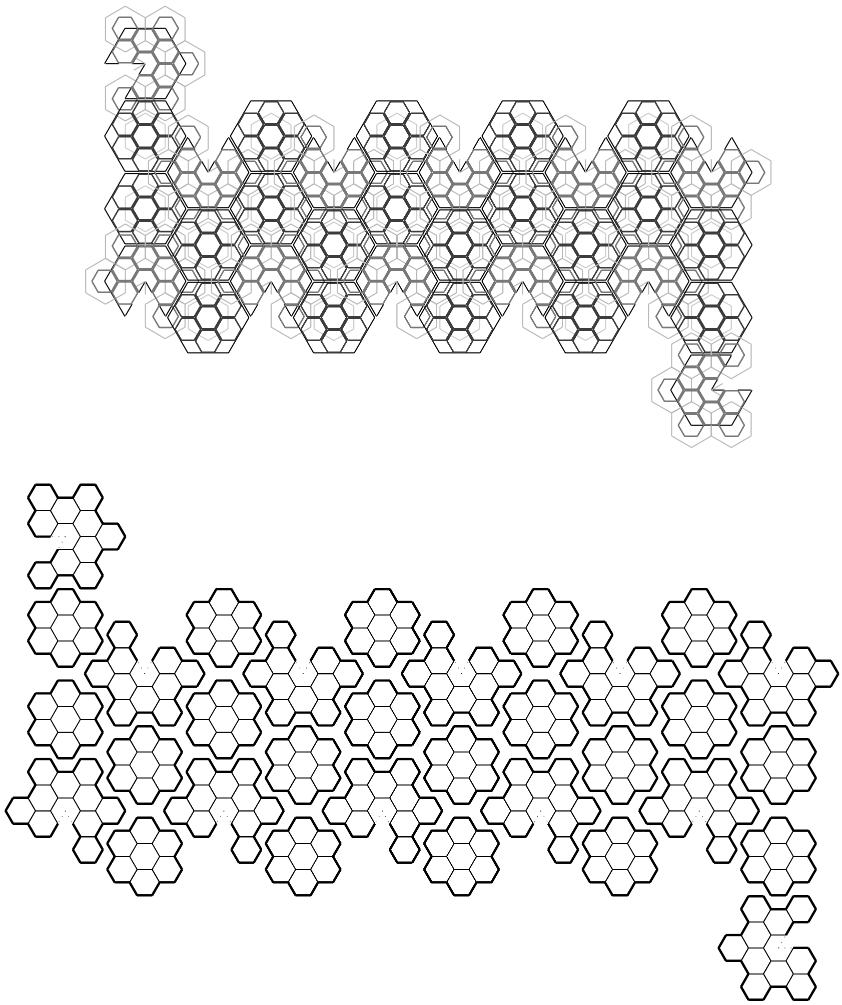

Figure 6. Level 2 – the hexagons generated from the subdivision of polygons in Figure 5.

3. PYXIS© array

This section begins with a precise definition of the PYXIS© multi-resolution sequence **P** of planar hexagonal grids that was introduced informally in the previous section. The definition is recursive, the grid at a given resolution defined in terms of the grids at the two previous lower resolutions. A few basic properties that follow from the definition are then listed, including a tree-like structure on the cells at all resolutions. The section concludes with an indexing scheme that assigns to each cell at resolution n a string of n digits from the set $\{0,1,2,3,4,5,6\}$. This indexing is a natural one in that it is compatible with the tree structure, as explained at the end of this section, and has an arithmetic, as explained in the next section. The indexing scheme is based on a representation theorem that is analogous to the representation of integers in base 3. This is further explained in Section 4.

It is convenient to represent each hexagonal cell in a grid by its center. The centers of the cells at a given resolution are a finite set of points of a hexagonal lattice in the plane. More precisely, a *two-dimensional lattice* L is the set of all integer linear combinations of two independent vectors in the plane R^2. The elements of the lattice are called *lattice points*. The Voronoi cell of a lattice point $\mathbf{x}$ in a two-dimensional lattice L is a set consisting of all points of R^2 which are at least as close to $\mathbf{x}$ as to any other lattice point of L. If the Voronoi cells are regular hexagons, then the lattice is called a *hexagonal lattice*. A finite, non-empty subset of a hexagonal lattice, or the corresponding set of Voronoi cells, will be called a *hexagonal array*. Throughout this paper we often refer to the lattice point and its Voronoi cell (hexagon) interchangeably.

In this paper, Z, R, and C denote the set of integers, real numbers, and complex numbers, respectively. If $\mathbf{u}$ and $\mathbf{v}$ are two linearly independent vectors in R^2, then $L := \{n_1\mathbf{u} + n_2\mathbf{v} : n_1, n_2 \in Z\}$ is a two-dimensional lattice and $\{\mathbf{u}, \mathbf{v}\}$ is called a *set of generators* of L. Let

$$\mathbf{u}_A = (1,0), \qquad \mathbf{v}_A = \left(-\frac{1}{2}, \frac{\sqrt{3}}{2}\right),$$

$$\mathbf{u}_B = \left(\frac{\sqrt{3}}{2}, \frac{1}{2}\right), \qquad \mathbf{v}_B = \left(-\frac{\sqrt{3}}{2}, \frac{1}{2}\right).$$

For $n \geq 1$, let $\rho = 1/\sqrt{3}$, and

$$\mathbf{u}_n = \begin{cases} \rho^n \mathbf{u}_A, & \text{if } n \text{ is odd,} \\ \rho^n \mathbf{u}_B, & \text{if } n \text{ is even,} \end{cases} \qquad \mathbf{v}_n = \begin{cases} \rho^n \mathbf{v}_A, & \text{if } n \text{ is odd,} \\ \rho^n \mathbf{v}_B, & \text{if } n \text{ is even,} \end{cases}$$

For $n \geq 1$, define the lattice

$$L_n = \{n_1\mathbf{u}_n + n_2\mathbf{v}_n : n_1, n_2 \in Z\}.$$

It is not hard to check that each L_n is a hexagonal lattice. For n odd, L_n is just a scaled copy of L_1, and for n even, L_n is a scaled copy of L_1 rotated 30° about the origin. It is also easy to check that the L_n are nested in the sense that, for all $n \geq 1$,

$$L_n \subset L_{n+1}.$$

Let $W_n = \{\omega_{n,1}, \ldots, \omega_{n,6}\}$ denote the six immediate neighbors of $\mathbf{0} := (0,0)$ in the lattice L_n. The six lattice points of W_n are ordered counterclockwise as shown in Figure 7 for both the even and the odd case. More precisely, the six points of W_n, in order, are $(\mathbf{u}_n + \mathbf{v}_n, \mathbf{v}_n, -\mathbf{u}_n, -\mathbf{u}_n - \mathbf{v}_n, -\mathbf{v}_n, \mathbf{u}_n)$ for both the even and odd cases.

For any lattice L and $\emptyset \neq X, Y \subseteq L$, we use the notation $X + Y := \{\mathbf{x} + \mathbf{y} \in L : \mathbf{x} \in X, \mathbf{y} \in Y\}$. The *PYXIS*© *array* $\mathbf{P}_n$ can now be defined recursively as follows.

Definition 3.1 Let $\mathbf{P}_0 = \mathbf{0}$, $\mathbf{P}_1 = W_1 \cup \{\mathbf{0}\}$ and, for any integer $n > 1$,

$$\mathbf{P}_n = \mathbf{P}_{n-1} \cup (\mathbf{P}_{n-2} + W_n). \tag{1}$$

The set $\mathbf{P}_n$ is called *the PYXIS*© *array at level n*.

Let h be any hexagon at level n centered at lattice point $\mathbf{x}$. According to the recursive definition of $\mathbf{P}_n$, there is a hexagon h' at level $n+1$ centered at the same lattice point $\mathbf{x}$. Call h' the *central child* of h. Also according to the definition, there

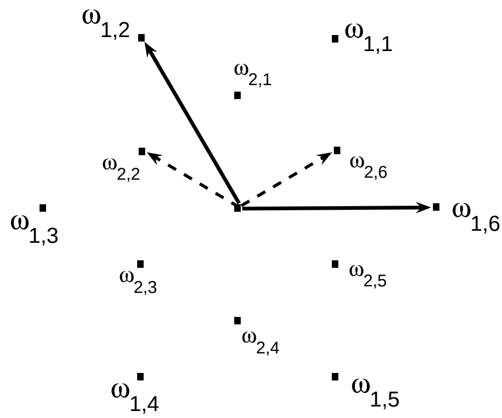

Figure 7. The generators of the lattices L_1 and L_2 and the lattice points contained in W_1 and W_2.

are six hexagons $h_1, h_2, \ldots, h_6$ in $\mathbf{P}_{n+2}$ centered at the lattice points $\mathbf{x}+W_{n+2}$. Call these the *vertex children* of h (see Figure 8). This provides a natural tree-like data structure on the PYXIS© cells.

Properties of P. Property 1 in the list below follows immediately from the definition of $\mathbf{P}_n$ and the facts that the L_n are nested and that $W_n \subset L_n$. Property 2 follows immediately from the definition of $\mathbf{P}_n$, and property 3 follows from the definition of L_n. Property 4 is easily verified by induction using the definition of $\mathbf{P}_n$.

1. $\mathbf{P}_n \subset L_n$ for $n \geq 1$.
2. The PYXIS© arrays are nested: $\mathbf{P}_0 \subset \mathbf{P}_1 \subset \mathbf{P}_2 \subset \ldots$.
3. The ratio of the area of a $\mathbf{P}_n$ hexagon to the area of a $\mathbf{P}_{n+1}$ hexagon is 3.
4. The number of lattice points in $\mathbf{P}_n$ is $\frac{1}{5}(3^{n+2} - (-2)^{n+2})$.

The PYXIS© indexing scheme, explained below, is based on the following representation theorem for the lattice points of $\mathbf{P}_n$.

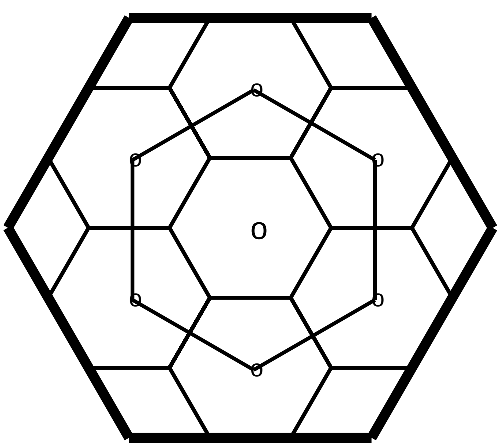

Figure 8. The vertex child and central children of a cell.

Theorem 3.2 *For any $n \geq 0$ and $\mathbf{a} \in \mathbf{P}_n$, there exist uniquely determined $\omega_i \in W_i \cup \{\mathbf{0}\}$ such that*

$$\mathbf{a} = \sum_{i=1}^{n} \omega_i, \tag{2}$$

and either $\omega_i = \mathbf{0}$ or $\omega_{i+1} = \mathbf{0}$ for each i satisfying $0 \leq i < n$.

Proof. Let S_n be the set of all points of the form $\mathbf{a} = \Sigma_{i=1}^{n} \omega_i$, where $\omega_i \in W_i \cup \{\mathbf{0}\}$ and either $\omega_i = \mathbf{0}$ or $\omega_{i+1} = \mathbf{0}$ for each i satisfying $0 \leq i < n$. The set S_{n-1} consists of all such sums $\Sigma_{i=1}^{n} \omega_i$, where $\omega_n = \mathbf{0}$, and $S_{n-2} + W_n$ consists of all such sums $\Sigma_{i=1}^{n} \omega_i$, where $\omega_{n-1} = \mathbf{0}$. Hence the sets S_n satisfy the same recurrence (1) as do the sets $\mathbf{P}_n$. Since it is easy to check that $S_n = \mathbf{P}_n$ for $n = 0,1$, the equality $S_n = \mathbf{P}_n$ holds for all n.

The uniqueness is proved by induction. It is easily checked for $n = 0,1$. Assume that $\Sigma_{i=1}^{n} \omega_i = \Sigma_{i=1}^{n} \omega_i'$. If $\omega_i = \omega_n'$, then, by induction, $\Sigma_{i=1}^{n-1} \omega_i = \Sigma_{i=1}^{n-1} \omega_i'$ implies that $\omega_i = \omega_n'$ for all i. If $\omega_n \neq \omega_n'$, consider two cases. If exactly one of ω_n or ω_n' is $\mathbf{0}$, say $\omega_n' = \mathbf{0}_i$, then, because the lattices L_i are nested, $\omega_n = \Sigma_{i=1}^{n-1} (\omega_i' - \omega_i) \in L_{n-1}$. But this is a contradiction because $\omega_n \notin L_{n-1}$. If neither ω_n nor ω_n' is $\mathbf{0}$, then, because no two consecutive ω_i (or ω_i') are non-zero, $\omega_n - \omega_n' = \Sigma_{i=1}^{n-2} (\omega_i' - \omega_i) \in L_{n-2}$. This is also a contradiction because $\omega_n - \omega_n' \notin L_{n-2}$. □

Theorem 3.2 can be used as follows to assign to each cell in $\mathbf{P}_n$ a label (address) that is a string of n digits from the set $\{0,1,2,3,4,5,6\}$. The expression $\mathbf{a} = \Sigma_{i=1}^{n} \omega_i$ in Theorem 3.2 will be called the *standard form* for $\mathbf{a}$ in $\mathbf{P}_n$. Recall that $W_n = \{\omega_{n,1}, \ldots, \omega_{n,6}\}$. Let $\omega_{n,0} = \mathbf{0}$ and $\overline{W}_n = \{\omega_{n,0}, \omega_{n,1}, \ldots, \omega_{n,6}\}$. So, in standard form,

$$\mathbf{a} = \sum_{i=1}^{n} \omega_{i,a_i},$$

where $\omega_{i,a_i} \in \overline{W}_i$ and $a_i \in \{0,1,2, \ldots ,6\}$. The string $a_1 a_2 \ldots a_n$ of integers in the standard form will be called the *label* of $\mathbf{a}$ in $\mathbf{P}_n$. In light of the obvious one-to-one correspondence between lattice points and Voronoi cells, the string $a_1 a_2 \ldots a_n$ also serves as the label of the Voronoi cell of $\mathbf{a} \in \mathbf{P}_n$. Note that, in the label of a point in $\mathbf{P}_n$, there are no two consecutive non-zero digits. It is easy to verify that the center hexagon of $\mathbf{P}_1$ is labeled 0 and the other six hexagons of $\mathbf{P}_1$ are labeled 1, 2, 3, 4, 5, 6 going counterclockwise. The PYXIS© array $\mathbf{P}_2$ consists of 13 hexagons labeled 00, 10, 20, 30, 40, 50, 60, 01, 02, 03, 04, 05 and 06. Figure 9 shows the labels of $\mathbf{P}_1$, $\mathbf{P}_2$, $\mathbf{P}_3$, $\mathbf{P}_4$, while Figure 10 shows the labels just at level 4 such that no two consecutive terms are non-zero. Then the representation theorem implies the following.

Corollary 3.3 *There is a bijection between $\mathbf{P}_n$ and the set of all strings of length n from the set $\{0,1,2,3,4,5,6\}$ such that no two consecutive terms are non-zero.*

The following result also follows directly from the definitions of $\mathbf{P}_n$ and its labels.

Corollary 3.4:

1. *If α is the label of a point in $\mathbf{P}_n$, then $\alpha\ 0$ is the label of its central child.*
2. *If α is the label of a point in $\mathbf{P}_n$, then $\alpha\ 0\ k$, $1 \leq k \leq 6$, are the labels of its six vertex children.*

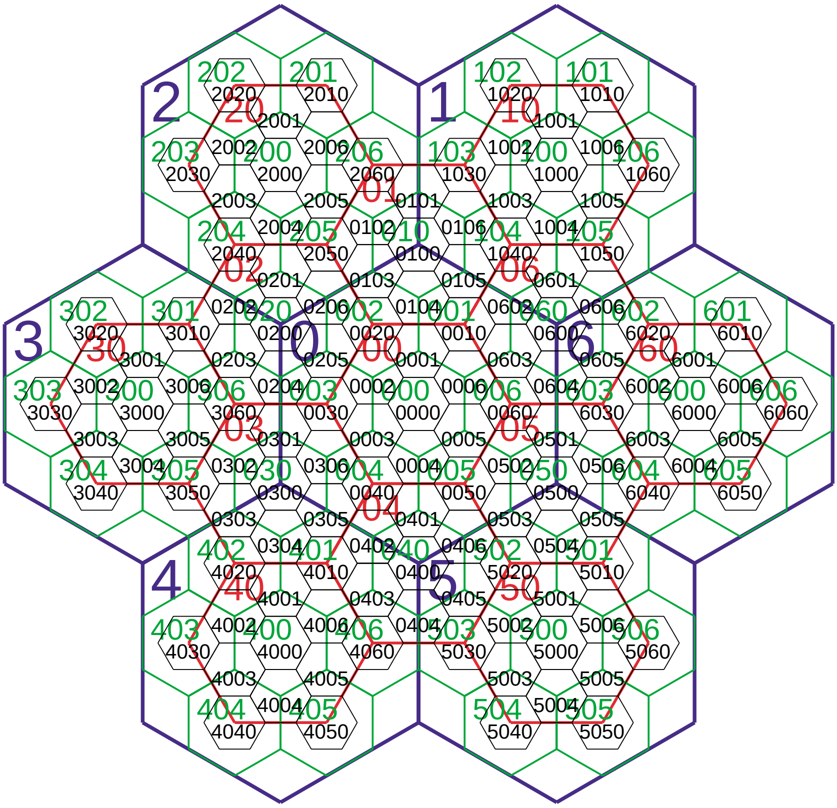

Figure 9. Labeled cells at levels 1 through 4 of the PYXIS© array.

In this section, the recursive definition of the arrays $\mathbf{P}_n$ led to a natural way to uniquely label each of its hexagonal cells. These results lead to an elegant tree-like data structure on the PYXIS© cells. The labeling method is further refined in the next section to yield an efficient algorithm for vector addition of two points in $\mathbf{P}_n$ in terms of their labels.

4. Addition algorithm

Just as the arithmetic of coordinates of points in a standard array is essential for data retrieval, the arithmetic for the labels of lattice points in a PYXIS© array is important for data retrieval on PYXIS© grids. Let Λ_n denote the set of all strings of length n from the set $\{0,1,2,3,4,5,6\}$ such that no two consecutive terms are non-zero. Given two lattice points $\mathbf{a},\mathbf{b} \in \mathbf{P}_n$ the goal is, in terms of their labels in Λ_n, to determine the vector sum $\mathbf{a}+\mathbf{b}$. This section begins with an informal explanation of the method, which is based on an equivalent version of the representation Theorem 3.2. This is followed by the full algorithm.

For $\mathbf{a} \in \mathbf{P}_n$ let $\lambda(\mathbf{a})$ denote the label of $\mathbf{a}$ in $\mathbf{P}_n$. Let $\lambda(\mathbf{a}) = a_1a_2 \ldots a_n$ and $\lambda(\mathbf{b}) = b_1b_2 \ldots b_n$. If $\mathbf{a}+\mathbf{b} \in \mathbf{P}_n$ and $\lambda(\mathbf{a}+\mathbf{b}) = c_1c_2 \ldots c_n$, then the label $c_1c_2 \ldots c_n$ is called the *sum* of the labels $a_1a_2 \ldots a_n$ and $b_1b_2 \ldots b_n$, and we write $c_1c_2 \ldots c_n = a_1a_2 \ldots a_n \oplus$

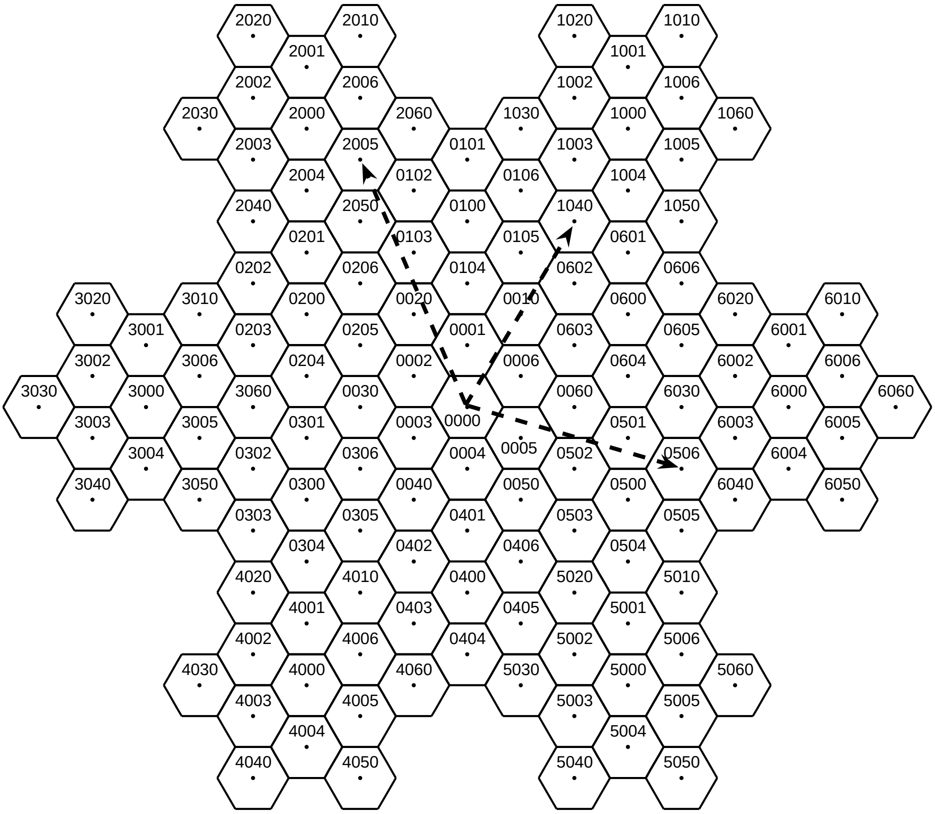

Figure 10. Labeled cells at level 4 of the PYXIS© array.

$b_1 b_2 \ldots b_n$ in Λ_n. For example, the three dashed vectors in Figure 10 show that $0506 \oplus 2005 = 1040$ in Λ_4. If $\mathbf{a}+\mathbf{b} \notin \mathbf{P}_n$, then we have an 'overflow'.

Table 1 is a partial table for addition in Λ_4. (Because it is obvious that $0000 \oplus abcd = abcd$ for any a,b,c,d, this is not included in the table.) A general algorithm for addition in the set Λ_n is given below, and Table 1 is used in that algorithm. Referring to the table, if $00a_1a_2 \oplus 00b_1b_2 = c_1c_2c_3c_4$, then c_1c_2 and c_3c_4 will be called the *carry* and the *remainder* of the addition, respectively.

By grouping terms into pairs in its standard form (2), we obtain the equivalent form for a point $\mathbf{a} \in \mathbf{P}_n$,

$$\mathbf{a} = \sum_{i=1}^{\lceil n/2 \rceil} \mathbf{w}_i 3^{-i},$$

where

$$\mathbf{w}_i = \omega_i + \omega_i',$$

for some $\omega_i \in \overline{W}_1$, $\omega_i' \in \overline{W}_2$. Note that, although $\omega_i + \omega_i' \in \overline{W}_1 + \overline{W}_2$, it cannot be just any element of $\overline{W}_1 + \overline{W}_2$ because, by the definition of the standard form, either ω_i or ω_i' (or both) must be $\mathbf{0}$. Hence there are exactly 13 possibilities for each $\mathbf{w}_i$ (including 00). Thus, the standard form for $\mathbf{P}_n$ is essentially a base 3 number system

Table 1. Partial addition table for **P**4.

$\oplus$	0001	0002	0003	0004	0005	0006	0010	0020	0030	0040	0050	0060
0001	0104	0020	0002	0000	0006	0010	0105	0103	0205	0003	0005	0603
0002	0020	0205	0030	0003	0000	0001	0104	0206	0204	0306	0004	0006
0003	0002	0030	0306	0040	0004	0000	0001	0205	0301	0305	0401	0005
0004	0000	0003	0040	0401	0050	0005	0006	0002	0306	0402	0406	0502
0005	0006	0000	0004	0050	0502	0060	0603	0001	0003	0401	0503	0501
0006	0010	0001	0000	0005	0060	0603	0602	0104	0002	0004	0502	0604
0010	0105	0104	0001	0006	0603	0602	1040	0100	0020	0000	0060	0600
0020	0103	0206	0205	0002	0001	0104	0100	2050	0200	0030	0000	0010
0030	0205	0204	0301	0306	0003	0002	0020	0200	3060	0300	0040	0000
0040	0003	0306	0305	0402	0401	0004	0000	0030	0300	4010	0400	0050
0050	0005	0004	0401	0406	0503	0502	0060	0000	0040	0400	5020	0500
0060	0603	0006	0005	0502	0501	0604	0600	0010	0000	0050	0500	6030
0100	0101	0102	0103	0104	0105	0106	1030	2060	2050	0020	0010	1040
0200	0201	0202	0203	0204	0205	0206	2050	2040	3010	3060	0030	0020
0300	0301	0302	0303	0304	0305	0306	0030	3060	3050	4020	4010	0040
0400	0401	0402	0403	0404	0405	0406	0050	0040	4010	4060	5030	5020
0500	0501	0502	0503	0504	0505	0506	6030	0060	0050	5020	5010	6040
0600	0601	0602	0603	0604	0605	0606	1050	1040	0010	0060	6030	6020

(radix system) using 13 digits. There would be redundancy (non-uniqueness of representation) if not for the requirement of no two consecutive non-zero digits. Theorem 1 guarantees unique representation. Exactly as for other familiar radix number systems, addition in $\mathbf{P}_n$ can be carried out by summing digits from right to left, and possibly 'carrying' a digit one place to the left. In our case, each of the 13 possible $\mathbf{w}_i$ are represented by a pair of digits (00,01,02,03,04,05,06,10,20,30,40, 50,60). Hence, addition is carried out two digits at a time instead of one digit at a time. Table 1 is the basic addition table for PYXIS©, exactly as the 10×10 addition table is the basic table for base 10 arithmetic. There is one glitch – namely it may happen that, by using the table, we arrive at two consecutive non-zero digits, for example 0320. In this case we can use Table 1 to convert the label to standard form: $0320 = 0300 \oplus 0020 = 3060$.

As an example, consider $001020 \oplus 000503 = (00|10|20) \oplus (00 \,|\, 05 \,|\, 00)$. We proceed from right to left in pairs, always using Table 1.

Stage 1: $20 \oplus 00 \rightarrow 0020 \oplus 0000 = 0020 = 00 \,|\, 20$. The remainder is 20 and the carry is 00. The sum to this point is 20.

Stage 2: $10 \oplus 05 \oplus 00$ (carry) $\rightarrow 0010 \oplus 0005 = 0603 = 06 \,|\, 03$. So the remainder is 03 and the carry is 06. The concatenated sum at this point (from Stages 1 and 2) is 0320, which is not in standard form. So we convert using Table 1: $0320 = 0300 \oplus 0020 = 3060$.

Stage 3: $00 \oplus 00 \oplus 06$ (previous carry) $= 06$. The sum at this point is now 063060. Again, it must be converted into standard form: $0630 = 0600 \oplus 0030 = 0010$. Note that when $0ab0$ is converted to standard form, Table 1 gives $0a \oplus b0 = c0d0$, in particular the rightmost digit is always 0. Therefore, no new pair of consecutive non-zero digits is introduced to the right. In our example, the final sum is 001060.

The general algorithm appears below, followed by some explanatory comments.

Algorithm 1: SUM ($a_1a_2 \ldots a_n$, $b_1b_2 \ldots b_n$)

Input: Two labels $a_1a_2 \ldots a_n \in \Lambda_n$ and $b_1b_2 \ldots b_n \in \Lambda_n$.
Output: The $SUM := a_1a_2 \ldots a_n \oplus b_1b_2 \ldots b_n$ in Λ_n, if it exists. Otherwise $SUM =$ overflow.

Step 1. If n is odd, append 0 to the end of each summand. So now each summand consists of $2m$ digits, for some m.

Step 2. Divide the digits into pairs as follows:

$$a_1a_2|a_3a_4|\ldots|a_{2m-1}a_{2m}$$
$$b_1b_2|b_3b_4|\ldots|b_{2m-1}b_{2m}$$

Denote the pairs by $A_1, \ldots, A_m$ and $B_1, \ldots, B_m$, respectively.
Initialize $C_m = 00$.

Step 3. For $k = m$ to 1 (right to left) do
Compute $00A_k \oplus 00B_k \oplus 00C_k$ as follows. If one of the summands is 0000, then use Table 1. Otherwise, first compute $D_k = 00A_k \oplus 00B_k$ using Table 1 – then recursively compute $00A_k \oplus 00B_k \oplus 00C_k = \mathrm{SUM}(00C_k, D_k)$.
Let R_k be the remainder and C_{k-1} the carry of $00A_k \oplus 00B_k \oplus 00C_k$.
If $R_k = 0a$ and $R_{k+1} = b0$, where $a,b \neq 0$, then use Table 1 to compute $0a00 \oplus 00b2 = c0d0$, and let $R_k = c0$ and $R_{k+1} = d0$.

Step 4. If $C_0 = 0a$ and $R_1 = b0$, where $a,b \neq 0$, then use Table 1 to compute $0a00 \oplus 00b0 = c0d0$, and let $C_0 = c0$ and $R_1 = d0$.

Step 5. If $C_0 \neq 00$, then $SUM =$ overflow.
Otherwise $SUM = R_1 \ldots R_m$, the concatenation of the R_k. If n is odd, the last digit in this concatenation is 0 – remove this 0.
Return SUM.

Concerning Step 1, by appending a 0 to the end of the label, the label of the central child is obtained. But the lattice point for the parent and central child is the same point. The 0 is removed in Step 5.

Concerning the first part of Step 3, note that, since $00C_k$ begins with 00, the algorithm does not perform a nested recursive call on SUM when SUM ($00C_k$, D_k) is performed. Hence the algorithm does not enter an infinite loop. Also note that any sum of three labels of the form $00a_1a_2 \oplus 00b_1b_2 \oplus 00c_1c_2$ lies in Λ_4; there is no 'overflow'. This can be proved formally, but can also be easily checked by referring to Table 1. Concerning the last part of Step 3, this puts the answer in standard form as explained prior to the algorithm. Step 4 is just to convert the leftmost digits to standard form.

Since the number of computations in each iteration in Step 3 is constant, the computational complexity of this algorithm is efficient, linear in n.

5. Discrete Fourier transform for PYXIS©

Because the discrete Fourier transform (DFT) is ubiquitous in data analysis and is an important tool in image processing, we consider the DFT on PYXIS© grids in this section. Its application to the PYXIS© arrays, however, is somewhat problematic.

The first issue is to formulate the DFT in the context of a lattice. The second, more difficult, issue is to apply it to the finite subset $\mathbf{P}_n$ of the hexagonal lattice. These are the topics addressed in this section.

In dimension 1, consider cells of unit length centered, say, at the points $0, \pm 1, \pm 2, \ldots$. An *image* can be thought of as a complex-valued function defined on a finite subset, say $\{0,1,2, \ldots, N-1\}$, of these points. Let $C^{[N]}$ denote the vector space of all such functions. The classical discrete Fourier transform (DFT) is the linear transformation $\mathcal{F}:C^{[N]} \to C^{[N]}$ defined by

$$(\mathcal{F}a)(k) = \sum_{j=0}^{N-1} a(j)e^{-2i(jk/N)}.$$

The set $S_N = \{0,1,2, \ldots, N-1\}$ can be regarded as a set of coset representatives of the quotient Z/NZ (i.e. residues modulo N). In fact, the DFT can be thought of as being defined on this quotient Z/NZ. Although any set of coset representatives can be used, the set S_N is particularly useful for practical applications.

Using the notion of the quotient lattice, the DFT can be extended to the two-dimensional hexagonal lattice (or, for that matter, to an arbitrary lattice in any dimension). A non-empty subset L_0 of a lattice L that is itself a lattice of the same dimension as L is called a *sublattice* of L. The *quotient* $G: = L/L_0$ is just the quotient of the lattices considered as Abelian groups. The *dual* L^* of a lattice L is defined by

$$L^* = \{\mathbf{s} \in R^2 : \langle \mathbf{r}, \mathbf{s} \rangle \in Z, \text{ for all } \mathbf{r} \in L\},$$

where $\langle \mathbf{r}, \mathbf{s} \rangle$ denotes the ordinary inner product of $\mathbf{r}$ and $\mathbf{s}$. Let $G^* : = L_0^*/L^*$. For an arbitrary lattice L and sublattice L_0, the DFT is defined as the linear transformation

$$\mathcal{F}:C^G \to C^{G^*},$$

given by

$$(\mathcal{F}a)(\bar{\mathbf{s}}) = \frac{1}{\sqrt{N}} \sum_{\bar{\mathbf{r}} \in G} a(\bar{\mathbf{r}})e^{-2i\langle \mathbf{r}, \mathbf{s} \rangle}, \tag{3}$$

for all $a \in C^G$ and all $\bar{\mathbf{s}} \in G^*$. Some properties of the DFT as defined above can be found in Zapata and Ritter (2000).

Consider the following geometric interpretation. For any finite subset $T \subseteq L$ and $\mathbf{x} \in L$, let $T_\mathbf{x} : = \mathbf{x} + T$. We say that T *tiles the lattice L by translations by the sublattice* L_0 if

$$\bigcup_{\mathbf{x} \in L_0} T_\mathbf{x} = L$$

and

$$T_\mathbf{x} \cap T_\mathbf{y} = \emptyset$$

whenever $\mathbf{x} \neq \mathbf{y}$. In this context, T is called a *tile*. Each tiling (tile) involved in this paper is a tiling (tile) by translations by a sublattice. It is easy to show that a subset $T \subset L$ is a tile if and only if T is a set of coset representatives of L/L_0 for some sublattice L_0. So, in Definition 3 of the DFT, a tile T can be taken as a set of coset representatives of the quotient group L/L_0. Hence, if T is not such a tile, the region T is not amenable to the DFT as defined in Equation (3). The following theorem, the somewhat complicated proof of which appears in Zheng (2007), shows that, for any integer $n > 2$, the nth level PYXIS© array $\mathbf{P}_n$ does not tile the underlying hexagonal lattice L_n. Hence we cannot apply the above definition of the DFT to $\mathbf{P}_n$.

Theorem 5.1 *For any $n > 2$, the nth level $\mathbf{P}_n$ of the PYXIS© array does not tile its underlying lattice L_n.*

Since the DFT cannot be directly applied to the PYXIS© array $\mathbf{P}_n$, we introduce another sequence of arrays that closely approximates the $\mathbf{P}_n$ and that is amenable to our formulation of the DFT. Recall from Section 2 that

$$\mathbf{u}_A = (1,0), \quad \mathbf{v}_A = \left(-\frac{1}{2}, \frac{\sqrt{3}}{2}\right), \quad \mathbf{u}_B = \left(\frac{\sqrt{3}}{2}, \frac{1}{2}\right), \quad \mathbf{v}_B = \left(-\frac{\sqrt{3}}{2}, \frac{1}{2}\right).$$

Let L_A be the lattice generated by $\mathbf{u}_A$ and $\mathbf{v}_A$, and similarly L_B the lattice generated by $\mathbf{u}_B$ and $\mathbf{v}_B$. Let $\mathfrak{R}_n^A$ be the subset of L_A that lies within the closed convex hull of the six points

$$\{j\mathbf{u}_A + k\mathbf{v}_A : (j,k) \in \{\pm(n,0), \pm(0,n), \pm(n,n)\},$$

and $\mathfrak{R}_n^B$ the subset of L_B that lies within the closed convex hull of the six points

$$\{j\mathbf{u}_B + k\mathbf{v}_B : (j,k) \in \{\pm(n,-n), \pm(2n,n), \pm(n,2n)\}.$$

The arrays $\mathfrak{R}_n^A$ and $\mathfrak{R}_n^B$ are hexagonal in shape, the case $n = 3$ shown in Figure 11(a) and (b), respectively. It has been proved by Vince and Zheng (2007) that the array $\mathfrak{R}_n^A$ is a set of coset representatives of the quotient of the hexagonal lattice L_A by a hexagonal sublattice. Likewise, $\mathfrak{R}_n^B$ is the set of coset representatives of the quotient of L_B by a hexagonal sublattice. We call a set of coset representatives of the quotient of two hexagonal lattices a *regular hexagonal* array.

Using the general method outlined at the beginning of this section, the DFT on $\mathfrak{R}_n^A$ and $\mathfrak{R}_n^B$ can be computed. Moreover, the paper of Vince and Zheng (2007) gives a detailed exposition of the DFT on regular hexagonal arrays. A particularly efficient method in that paper computes the two-dimensional hexagonal DFT by converting it to the one-dimensional standard DFT.

It remains to show the relationship between the regular hexagonal arrays and the PYXIS© arrays. The following theorem states that, up to a scaling factor, $\mathbf{P}_n$ can be tightly embedded into a regular hexagonal array. In Figure 12, the solid hexagons are cells of $\mathbf{P}_4$, and the dashed hexagons are the remaining cells of the corresponding level of the regular hexagonal array. To be precise, define a scaled version of the regular hexagonal array as follows. Let $k := k(n) = \frac{1}{2}(3^n - 1)$ and $\rho = 1/\sqrt{3}$. Then for $n \geq 1$ define

$$\mathbf{R}_{2n-1} = \rho^{2n-1}\mathfrak{R}_k^A, \quad \mathbf{R}_{2n} = \rho^{2n}\mathfrak{R}_k^B.$$

The following properties 1–3 are easily checked for all n, and property 4 is derived in Vince and Zheng (2007), and is not a difficult calculation.

1. $\mathbf{R}_{\mathrm{n}} \subset L_n$,
2. $\mathbf{R}_n \subset \mathbf{R}_{n+1}$,

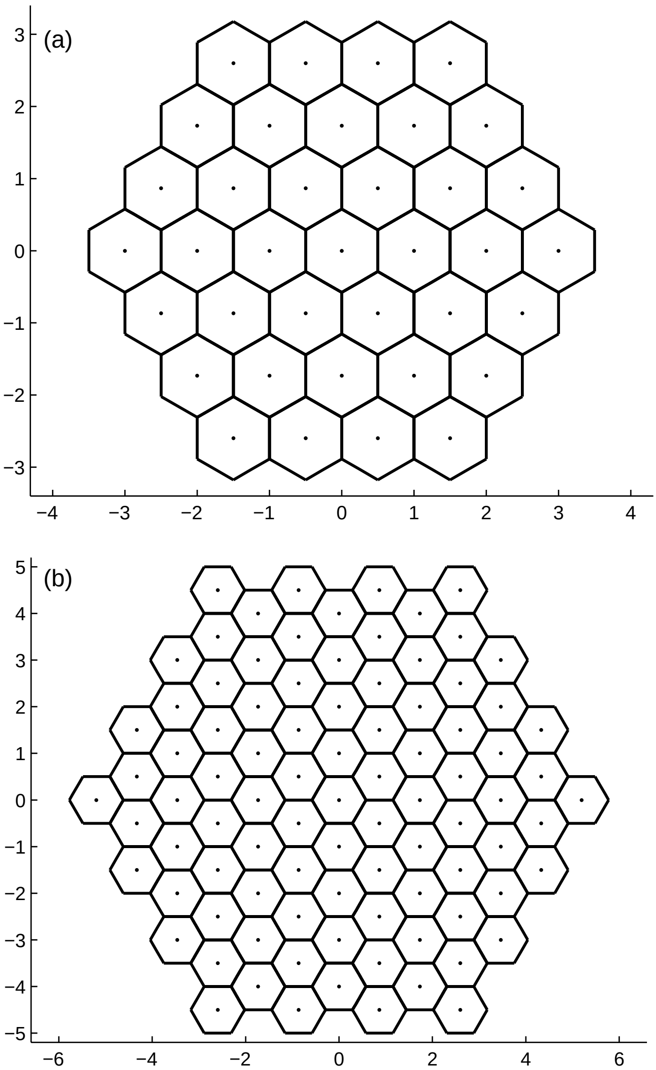

Figure 11. The regular hexagonal array $\mathfrak{R}_3^A$ (a) and $\mathfrak{R}_3^B$ (b).

3. both $\mathbf{R}_{2n+1}$ and $\mathbf{R}_{2n}$ consist of all points contained in the closed convex hull of the six points $X_n = \{k\omega : \omega \in W_{2n-1}\}$,
4. $|\mathfrak{R}_n^A| = 3n^2 + 3n + 1$ and $|\mathfrak{R}_n^B| = 9n^2 + 3n + 1$.

Statements 1 and 2 in the following theorem indicate that each PYXIS© array is contained in a particular regular hexagonal array of type $\mathbf{R}_n$, but in no coarser (scaled) regular hexagonal array of type $\mathfrak{R}^A$ or $\mathfrak{R}^B$. Hence statements 2 and 3 of the theorem indicate that the embedding of the PYXIS© array into a regular hexagonal array in statement 1 is tight.

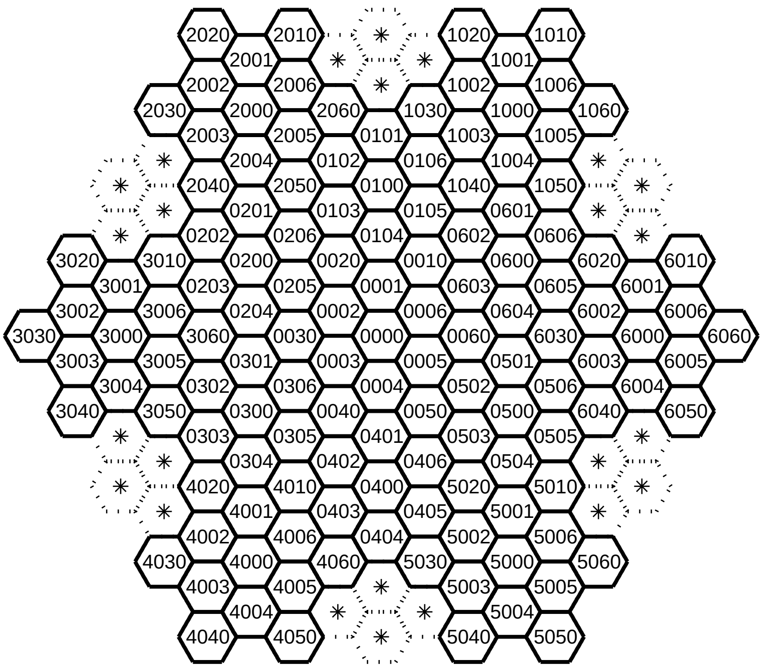

Figure 12. Array $\mathbf{P}_4$ embedded in the corresponding level of the regular hexagonal array.

Theorem 5.2:

1. *For all* $n \geq 1$, *we have* $\mathbf{P}_n \subset \mathbf{R}_n$.
2. *For* $k < \frac{1}{2}(3^n - 1)$, *the array* $\mathbf{P}_{2n-1}$ *is not a subset of the array* $\rho^{2n-1}\Re_k^A$ *and* $\mathbf{P}_n$ *is not a subset of* $\rho^{2n}\Re_k^B$.
3. *If* $|\mathbf{P}_n|$ *and* $|\mathbf{R}_n|$ *denote the number of lattice points in* $\mathbf{P}_n$ *and* $\mathbf{R}_n$, *respectively, then*

$$\lim_{n\to\infty} \frac{|\mathbf{P}_n|}{|\mathbf{R}_n|} = \frac{4}{5}.$$

Proof. Let $\omega \in W_{2n-1}$ and let $\vec{L}$ be the ray directed from the origin through ω. We first show by induction that $\mathbf{P}_{2n-1}$ contains the point $k\omega$ but no point on $\vec{L}$ past $k\omega$. The statement is clearly true for $n = 1$. By the definition of the PYXIS© array

$$\mathbf{P}_{2n-1} = \mathbf{P}_{2n-2} \cup (\mathbf{P}_{2n-3} + W_{2n-1}) = (\mathbf{P}_{2n-2} \setminus \mathbf{P}_{2n-3}) \cup \mathbf{P}_{2n-3} \cup (\mathbf{P}_{2n-3} + W_{2n-1}).$$

The set $\mathbf{P}_{2n-2} \setminus \mathbf{P}_{2n-3} \subset L_{2n-2} \setminus L_{2n-3}$ contains no points on $\vec{L}$. By the induction hypothesis, the set $\mathbf{P}_{2n-3}$ contains the point $[(3^{n-1} - 1)/2](3\omega)$ but no point on $\vec{L}$ past this point. Therefore, $\mathbf{P}_{2n-3} + W_{2n-1} \subset L_{2n-3} + W_{2n-1}$ contains $[(3^{n-1} - 1)/2](3\omega) + \omega = k\omega$ but no point on $\vec{L}$ past this point. A similar proof shows that $\mathbf{P}_{2n}$ contains the point $k\omega$ but no point on $\vec{L}$ past $k\omega$. Statement 2 of the theorem is now proved.

Since $\mathbf{P}_{2n-1}$ and $\mathbf{P}_{2n}$ both contain the set of six points X_n, to prove statement 1 of the theorem, it is sufficient to show that both $\mathbf{P}_{2n-1}$ and $\mathbf{P}_{2n}$ are contained in the convex hull $C_{2n-1} = C_{2n}$ of X_n. To do this, two facts are needed: $C_n \subseteq C_{n+1}$ for all n follows from properties 2 and 3 preceding the statement of the theorem, and $C_{2n-3} + \mathrm{conv}(W_{2n-1}) \subseteq C_{2n-1}$ is easily checked, where conv denotes the convex hull. The proof now proceeds by induction, the first case being immediate. For the odd case:

$$\mathbf{P}_{2n-1} = \mathbf{P}_{2n-2} \cup (\mathbf{P}_{2n-3} + W_{2n-1}) \subset C_{2n-2} \cup (C_{2n-3} + W_{2n-1}) \subseteq C_{2n-1},$$

where the second to last inclusion is by the induction hypothesis and the last inclusion by the facts above. For the even case:

$$\begin{aligned}\mathbf{P}_{2n} = \mathbf{P}_{2n-1} \cup (\mathbf{P}_{2n-2} + W_{2n}) &\subset C_{2n-1} \cup (C_{2n-2} + \mathrm{conv}(W_{2n})) \\ &\subseteq C_{2n-1} \cup (C_{2n-3} + \mathrm{conv}(W_{2n-1})) \subseteq C_{2n-1} = C_{2n},\end{aligned}$$

the second to last inclusion because $C_{2n-2} = C_{2n-3}$ and $\mathrm{conv}(W_{2n}) \subset \mathrm{conv}(W_{2n-1})$.

Consider statement 3 of the theorem. By property 4 of the PYXIS© array in Section 3, we have $|\mathbf{P}_{2n-1}| = \frac{1}{5}(3^{2n+1} - (-2)^{2n+1})$. Also by property 4 of hexagonal arrays in this section

$$|\mathbf{R}_{2n-1}| = |\Re_k^A| = 3k^2 + 3k + 1 = \frac{3}{4}(3^n - 1)^2 + \frac{3}{2}(3^n - 1) + 1 = \frac{1}{4}(3^{2n+1} + 1).$$

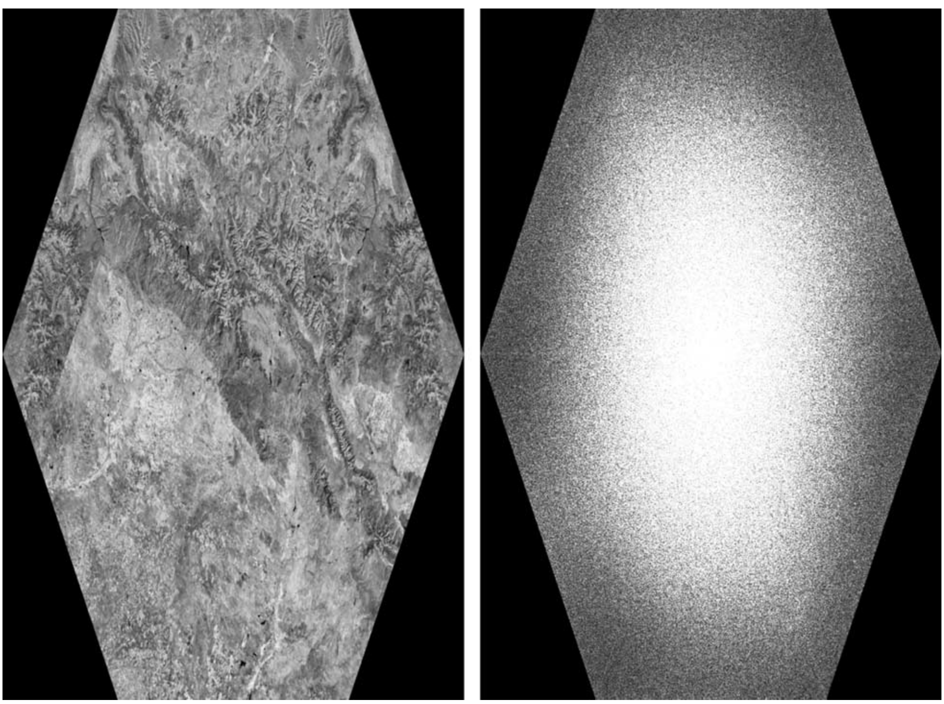

Figure 13. The Fourier transform. An image, on the left, on a regular hexagonal array. The right figure shows the frequencies of the left figure.

Therefore,

$$\lim_{n\to\infty}\frac{|\mathbf{P}_{2n-1}|}{|\mathbf{R}_{2n-1}|}=\lim_{n\to\infty}\frac{\frac{1}{5}(3^{2n+1}-(-2)^{2n+1})}{\frac{1}{4}(3^{2n+1}+1)}=\frac{4}{5}.$$

A similar argument holds in the even case. □

Using the notion of the quotient lattice, the DFT has been formulated in this section for certain finite subsets of the hexagonal lattice L. Such a subset must tile L by translations by a sublattice. For $n > 2$ the PYXIS© array $\mathbf{P}_n$, however, does not tile its underlying hexagonal lattice L_n by translations. To circumvent this problem, we have constructed another sequence of arrays, the regular hexagonal arrays $\mathbf{R}_n$, that do tile L_n by translations and into which the arrays $\mathbf{R}_n$ can be very closely embedded in the sense of Theorem 5.2. Our formulation of the DFT can be efficiently applied to $\mathbf{R}_n$. As shown in Figures 13 and 14, the DFT on a regular hexagonal array performs well in transforming a certain patch of image on the PYXIS© DGG.

6. Conclusion

ISEA3H is a multi-resolution, aperture 3, discrete global grid based on the Snyder equal area projection of a certain sequence of basically hexagonal subdivisions of the

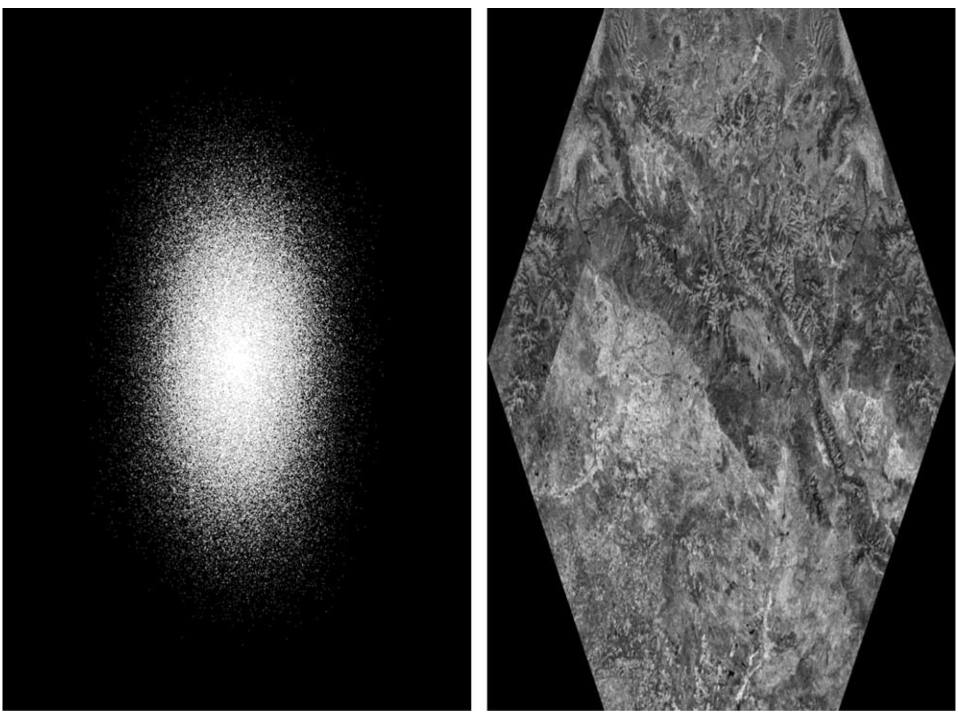

Figure 14. The inverse Fourier transform. The left figure shows the high frequencies in Figure 13 by cutting off the low frequencies. The right figure is the image obtained from the inverse Fourier transform of the left figure.

icosahedron. The PYXIS© digital Earth reference model is based on a partitioning of ISEA3H at each resolution into 32 pieces, each piece the projection of a finite, planar, hexagonal grid. The sequence of such planar grids is denoted $\mathbf{P}_n$, $n \geq 1$, in this paper. The research undertaken in this paper is foundational, namely

1. to provide a mathematical definition of the PYXIS© grids $\mathbf{P}_n$ and a precise description of the unique labeling of the cells of $\mathbf{P}_n$ by strings of n digits from the set {0,1,2,3,4,5,6}. This is essential to further research and to the development of algorithms,
2. to provide an efficient algorithm for the basic task of vector addition in $\mathbf{P}_n$, and
3. to provide an efficient method to perform the discrete Fourier transform on the grids $\mathbf{P}_n$.

Concerning item 1, a definition is given by the recursive formula (1) in Section 3, and the indexing, which is analogous to a base 3 radix system for the integers, is described in Sections 3 and 4. Item 2 is done in terms of the cell labels in Section 4 with linear computational complexity in n. Concerning item 3, the DFT is generalized in Section 5 from intervals in dimension 1 to two-dimensional 'tiles' in the hexagonal lattice. Although $\mathbf{P}_n$ is not a tile for $n > 2$, a small number of cells from the arrays surrounding $\mathbf{P}_n$ in the tessellation of the sphere can be added to $\mathbf{P}_n$ so that the DFT can be computed efficiently on the slightly extended array.

Acknowledgements

The authors would like to thank the team at PYXIS Innovation Inc. for valuable conversations prior to the writing of this paper.

Notes on contributors

Andrew Vince is a professor of mathematics at the University of Florida, USA. He has held visiting positions at Massey University, New Zealand, Dokuz Eylul University, Turkey, University of Kaiserslautern, Germany, Makerere University, Uganda, and Chancellor College, Malawi. His interest lies in discrete mathematics -combinatorics, graph theory, discrete and combinational geometry.

Xiqiang Zheng received his PhD degree from University of Florida in 2007, and then became an assistant professor of Voorhees College located at Denmark of South Carolina, USA. His research interests include applied mathematics, image processing, and pattern recognition. He is a member of IEEE Geoscience and Remote Sensing Society as well as the Society for Industrial and Applied Mathematics.

References

Ahuja, N., 1983. On approaches to polygonal decomposition for hierarchical image representation. *Computer Vision, Graphics, and Image Processing*, 24 (2), 200–214.

Anterrieu, E., Waldteufel, P., and Lannes, A., 2002. Apodization functions for 2-D hexagonally sampled synthetic aperture imaging radiometers. *IEEE Transactions on Geoscience and Remote Sensing*, 40 (12), 2531–2542.

Baumgardner, J.R. and Frederickson, P.O., 1985. Icosahedral discretization of the two-sphere. *SIAM Journal on Numerical Analysis*, 22 (6), 1107–1115.

Brodzik, M.J. and Knowles, K.W., 2002. EASE-Grid: a versatile set of equal-area projections and grids. *In*: M. Goodchild, ed. *Discrete global grids*. National Center for Geographic Information & Analysis.

Camps, A., *et al.*, 1997. The processing of hexagonally sampled signals with standard rectangular techniques: aApplication to 2-D large aperture synthesis interferometric radiometers. *IEEE Transactions on Geoscience and Remote Sensing*, 35 (1), 183–190.

Carr, D.B., Olsen, A.R., and White, D., 1992. Hexagon mosaic maps for the display of univariate and bivariate geographical data. *Cartography and Geographic Information Systems*, 19 (4), 228–236.

Chen, J., Zhao, X., and Li, Z., 2003. An algorithm for the generation of Voronoi diagrams on the sphere based on QTM. *Photogrammetric Engineering and Remote Sensing*, 69 (1), 79–90.

Dudgeon, D.E. and Mersereau, R.M., 1984. *Multidimensional digital signal processing*. Englewood Cliffs, NJ: Prentice Hall.

Goodchild, M.F. and Shiren, Y., 1992. A hierarchical spatial data structure for global geographic information systems. *Computer Vision, Graphics, and Image Processing*, 54 (1), 31–44.

Kidd, R., 2005. NWP discrete global grid systems. *ASCAT soil moisture report series* [online]. Vienna, Austria: Institute of Photogrammetry and Remote Sensing, Vienna University of Technology. Available from: www.ipf.tuwien.ac.at/radar/ascat/report_series/04_Discrete%20Global%20Grid%20Systems_2.2.pdf [Accessed February 2008].

Kitto, W. and Wilson, D.C., 1991. An isomorphism between the 7-adic integers and a ring associated with a hexagonal lattice. *Applicable Algebra in Engineering, Communication, and Computing*, 2 (2), 105–118.

Kitto, W.Z., Vince, A., and Wilson, D.C., 1994. An isomorphism between the p-adic integers and a ring associated with a tiling of N-space by permutohedra. *Discrete Applied Mathematics*, 52 (1), 39–51.

Lee, M. and Samet, H., 1998. Traversing the triangle elements of an icosahedral spherical representation in constant time. *In*: *Proceedings of the 8th international symposium on spatial data handling*. Burnaby, B.C.: International Geographical Union, 22–33.

Lucas, D., 1979. A multiplication in N-space. *Proceedngs of the American Mathematical Society*, 74 (1), 1–8.

Middleton, L. and Sivaswamy, J., 2005. *Hexagonal image processing*. London: Springer.

Peterson, P., 2003. Close-packed, uniformly adjacent, multiresolutional, overlapping spatial data ordering. International Patent Application, the PYXIS Innovation Inc., Canada.

PYXIS Innovation Inc., 2006. *Mathematics for a new grid system* [online]. Available from: www.pyxisinnovation.com [Accessed November 2008].

Sahr, K., White, D., and Kimmerling, A.J., 2003. Geodesic discrete global grid systems. *Cartography and Geographic Information Science*, 30 (2), 121–134.

Snyder, J., 1992. An equal-area map projection for polyhedral globes. *Cartographica*, 29, 10–21.

Szalay, A.S., *et al.*, 2005. Indexing the sphere with the hierarchical triangular mesh. Technical report, Microsoft Research.

Tong, X., *et al.*, 2007. The subdivision of partial geo-grid based on global geo-grid frame. *In*: *The 5th ISPRS workshop on DMGISs*, Urumchi, China.

Vince, A., 2006. Indexing the aperture 3 hexagonal discrete global grid. *Journal of Visual communication and Image Representation*, 17, 1227–1236.

Vince, A. and Zheng, X., 2007. Computing the discrete Fourier transform on a lattice. *Journal of Mathematical Imaging and Vision*, 28 (2), 125–133.

Zapata, J.L. and Ritter, G.X., 2000. Fast Fourier transform for hexagonal aggregates. *Journal of Mathematical Imaging and Vision*, 12 (3), 183–197.

Zheng, X., 2007. *Efficient Fourier transforms on hexagonal arrays*. Dissertation (PhD). University of Florida.